Elevated Curie temperature and half-metallicity in the ferromagnetic semiconductor La$_x$Eu$_{1-x}$O

Pedro M. S. Monteiro,[1,*] Peter J. Baker,[2] Nicholas D. M. Hine,[1,3] Nina-J. Steinke,[2] Adrian Ionescu,[1] Joshaniel F. K. Cooper,[2] Crispin H. W. Barnes,[1] Christian J. Kinane,[2] Zaher Salman,[4] Andrew R. Wildes,[5] Thomas Prokscha,[4] and Sean Langridge[2,†]

[1]*Cavendish Laboratory, Physics Department, University of Cambridge, Cambridge CB3 0HE, United Kingdom*
[2]*ISIS Facility, STFC Rutherford Appleton Laboratory, Harwell Science and Innovation Campus, Oxon, OX11 0QX, United Kingdom*
[3]*Department of Physics, University of Warwick, Coventry, CV4 7AL, United Kingdom*
[4]*Laboratory for Muon-Spin Spectroscopy, Paul Scherrer Institut, CH-5232 Villigen, Switzerland*
[5]*Institut Laue-Langevin, 6 rue Jules Horowitz, Boîte Postale 156, 38042 Grenoble Cedex 9, France*

Here we study the effect of La-doping in EuO thin films using superconducting quantum interference device magnetometry, muon spin rotation (μSR), polarized neutron reflectivity (PNR), and density functional theory (DFT). The μSR data shows that the La$_{0.15}$Eu$_{0.85}$O is homogeneously magnetically ordered up to its elevated T_C. It is concluded that bound magnetic polaron behavior does not explain the increase in T_C and an Ruderman-Kittel-Kasuya-Yosida-like (RKKY-like) interaction is consistent with the μSR data. The estimation of the magnetic moment by DFT simulations concurs with the results obtained by PNR, showing a reduction of the magnetic moment per La$_x$Eu$_{1-x}$O for increasing lanthanum doping. This reduction of the magnetic moment is explained by the reduction of the number of Eu-4f electrons present in all the magnetic interactions in EuO films. Finally, we show that an upwards shift of the Fermi energy with La or Gd doping gives rise to half-metallicity for doping levels as high as 3.2%.

PACS number(s): 75.50.Pp, 75.70.Ak, 75.30.Et, 76.75.+i

I. INTRODUCTION

Ferromagnetic semiconductors are attracting great interest for spintronic applications [1–3]. However, their technological impact is limited by their low Curie temperature (T_C). Therefore, it is paramount to find strategies to increase their T_C while maintaining their semiconductorlike character. In the group of ferromagnetic semiconductors, EuO with a T_C of 69 K has long been considered an archetypal model system since the exchange interaction is well approximated by the Heisenberg model [4,5]. EuO has a magnetic moment of $\sim 7\mu_B$ per Eu^{2+} atom [6] and a band gap of 1.12 eV at room temperature [7]. One of the most remarkable properties of EuO is the Zeeman splitting of the Eu-5d states below 69 K due to the influence of the Eu-4f states, causing a conduction band splitting of about 0.6 eV [8]. This high spin splitting energy when coupled with low n-doping was proven to transform EuO into a half-metal system [2,9]. Furthermore, the high localization of the Eu-4f electrons, which mediate the magnetic interactions, renders it convenient to study the exchange interaction phenomena.

There are several ways of increasing the T_C of EuO. The first is by altering the stoichiometry of EuO, e.g., introducing oxygen deficiency into EuO as we have recently shown [5,6,10]. The second is by applying strain [11], consequently changing the lattice parameter of the EuO system. However, first-principles calculations indicate that the band gap closes at 5% of isotropic stress and 6% biaxial strain [12]. The third and most promising mechanism to increase the T_C is by doping EuO with other elements. In the group of the lanthanide dopants gadolinium has shown to increase the T_C to as much as 170 K for a 4% doping concentration [13,14].

It was claimed recently by Miyazaki *et al.* [15] that a lanthanum doping concentration of 10% increased T_C to 200 K, while previous work published by Schmehl *et al.* [2] reported a maximum increase of the T_C to 118 K for 1% lanthanum doping. The latter authors also stated that no further increase in T_C occurred for higher doping levels. Previous measurements have also showed a T_C of 104 K for a 2% La-doping sample [16]. This elevation of T_C is believed to be caused by the donation of one 5d electron by the La atom into the conduction band strengthening thereby the magnetic interaction between the Eu-Eu next-nearest-neighbor atoms [16–18].

In a previous publication we studied the effect of n-type doping via oxygen deficiency on EuO thin films using μSR [5]. We have shown that the results for highly oxygen deficient films were incompatible with the bound magnetic polarons (BMP) [19] theory and that the Ruderman-Kittel-Kasuya-Yosida-like (RKKY-like) interaction is the only known model compatible with our data [20].

Here we study the effect of La-doping in EuO thin films; in particular, how the doping affects its magnetic moment and how the magnetic order persists above 69 K. This was done by probing the underlying physics by μSR, polarized neutron reflectivity (PNR), and superconducting quantum interference device (SQUID) magnetometry measurements. We have also used density functional theory (DFT) to draw a theoretical picture of how the La-doping changes the band structure. We also argue theoretically that the increase in doping changes the half-metallic behavior of the films.

The paper is organized as follows: we provide a description of the sample deposition and magnetometry (Sec. II), then use a local probe to address the exchange mechanism (Sec. III). In the second half of the paper we use density functional theory (Sec. IV) and supporting experimental data (Sec. V) to describe the half-metallicity in La$_x$Eu$_{1-x}$O and finish with some conclusions on the effect of doping (Sec. VI).

*pmdsm2@cam.ac.uk
†sean.langridge@stfc.ac.uk

II. SAMPLE DEPOSITION AND MAGNETOMETRY

The polycrystalline samples were deposited at 400 °C using a CEVP magnetron sputtering system with a base pressure of 5×10^{-9} Torr. Co-deposition was performed using three targets: a 99.99% pure Eu_2O_3, a 99.9% pure Eu, and a 99.9% pure La target. The deposition was performed by fixing the Eu_2O_3 flux and by keeping the total flux from the Eu and La constant. The La-doping was controlled by changing the relative flux between Eu and La. The growth was performed in an Ar^+ plasma at a pressure of 2 mTorr with a flow rate of 14 SCCM (where SCCM denotes cubic centimeter per minute at STP). The substrates used were Si(001). A SiO_2 layer was deposited between the substrate and the $La_xEu_{1-x}O$ film and another on the top as a capping layer to prevent further oxidation of the film. We deposited 10%, 15%, and 20% La-doped EuO samples.

The SQUID magnetometry measurements were performed in a Quantum Design MPMS 2 system. Each sample was cooled in a field of 50 Oe to 5 K followed by the $M(H)$ measurements at increasing temperatures. Finally each sample was cooled at zero field and the temperature dependent measurements where performed at different fields.

Figure 1 shows the SQUID data for the 15% La-doped EuO sample. The hysteresis curve shows a coercive field of 75 Oe compared to 54 Oe for the pristine EuO sample reported in Ref. [5]. The inset shows the bulk moment obtained at different saturation fields. The inset of Fig. 1 also shows the development of a clear ferromagnetic phase below 96 K, with a paramagnetic response above this temperature. The decrease of the coercivity with temperature is shown in Fig. 2. Similar measurements of the 10% and 20% samples find a T_C of about 94 and 84 K, respectively. The lower value for the 20% La-doped sample is due to disorder and the formation of impurities. The paramagnetic susceptibility is well described by the Curie-Weiss law and we used this to determine T_C.

FIG. 2. (Color online) Coercivity as a function of temperature for the 15% La-doped EuO sample.

The variation of the T_C obtained for different La-doping concentrations is shown in Fig. 3. There we compare the results found in the literature with the results we obtained in our samples. The value of the T_C presented in this paper is close to the values obtained by Schmehl *et al.* [2] and Vigren [16]. However, the result obtained by Miyazaki *et al.* [15] for a 10% La-doping concentration is significantly different from the value of 96 K we have obtained for a sample with the same doping concentration.

III. MAGNETIC SPATIAL HOMOGENEITY

The elevated Curie temperature of the EuO system has attracted considerable attention with several models being

FIG. 1. (Color online) Temperature dependent SQUID data for the 15% La-doped EuO sample. The inset shows the temperature dependence of the magnetic moment. The moment was normalized by the PNR results at 5 K.
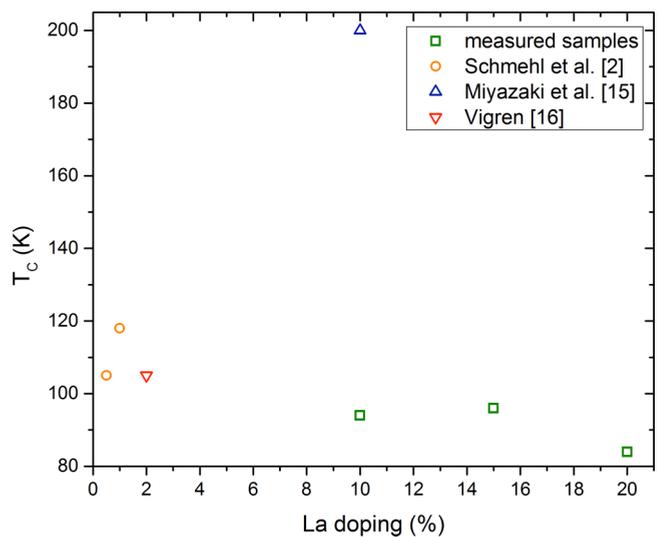
FIG. 3. (Color online) Variation of the T_C with La-doping. The samples measured by Schmehl *et al.* [2] and Miyazaki *et al.* [15] correspond to single crystal films, while the sample measured by Vigren [16] corresponds to a bulk crystal.
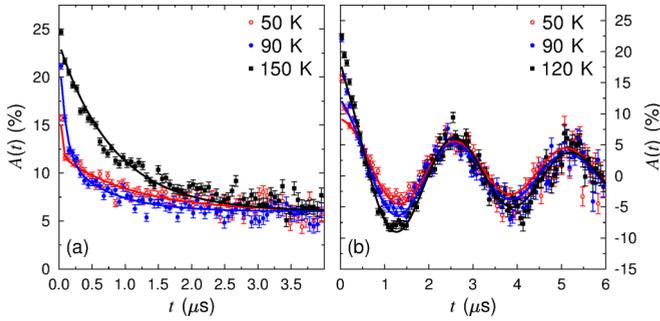
FIG. 4. (Color online) Raw muon data for the $La_{0.15}Eu_{0.85}O$ sample: (a) Zero-field measurements with the fits to Eq. (1). (b) Weak transverse field measurements with the fits to Eq. (2).

invoked to describe this behavior [19,20]. Low-energy muon measurements have been shown to be a highly effective local probe of the magnetism of such systems [5]. Our measurements were performed at the Paul Scherrer Institute, Switzerland, in zero applied field (ZF) and weak transverse field (wTF = 28.2 G) configurations, where muons were implanted into the film at various energies between 6 and 14 keV. In muon spin rotation (μSR) experiments [21] spin polarized positive muons are implanted into the sample, where they stop rapidly at interstitial sites of high electron density, and their spin direction evolves in the magnetic field at their stopping site. Each implanted muon decays with a lifetime of 2.2 μs emitting a positron preferentially in the direction of its spin at the time of decay. The evolution of their spin polarization as a function of time is determined by measuring the direction of the emitted positrons. In low-energy muon experiments [22–24], accelerating electric fields are used to control the implantation depth of the muons after they have passed through a cryogenic moderator. Example data are shown in Fig. 4. The lack of clear oscillations below T_C in ZF, compared with the data for bulk EuO obtained by Blundell *et al.* [21], may be due to small variations in the internal fields caused by a distribution of grain boundaries and defects in the film. This was also evident in our previous measurements of EuO_{1-x} [5].

We described the ZF data using the function [5]

$$A(t) = A_1 \exp(-\Lambda t) + A_2 \exp(-\lambda t) + A_{bg}, \quad (1)$$

where the sum of A_1 and A_2 (17.5%), and the background contribution A_{bg} (6%) are fixed by the geometry of the spectrometer and sample. The first term, describing the fast relaxation Λ, is found to be zero above T_C and represents an incoherent precession of muons about fields perpendicular to their spin polarization. This relaxation rate Λ, shown in Fig. 5(a), will therefore vary with the size of those fields and gives us some insight into the magnetic order parameter, albeit far more limited than a well-defined oscillation frequency. This change in Λ exhibits a similar temperature dependence to the magnetization recorded in our bulk measurements, fully consistent with following a ferromagnetic order parameter by both techniques. The second term describes a slow relaxation of muon spins, λ, which below T_C we can attribute to fluctuations of magnetic fields parallel to the muon spin polarization and above T_C is caused by paramagnetic spin fluctuations. Figure 5(b) shows that there is a small peak in λ
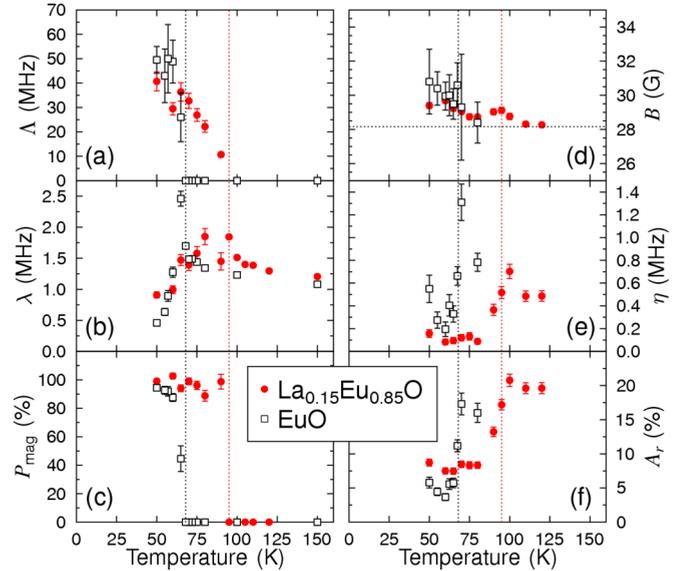
FIG. 5. (Color online) Fitted parameters for the zero-field muon data [(a)–(c)] and weak transverse field data [(d)–(f)]: (a) Fast relaxation rate, Λ. (b) Slow relaxation rate, λ. (c) Static magnetic volume fraction, P_{mag}. (d) Magnetic field, B, experienced by the implanted muons. (e) Relaxation rate, η. (Square-root exponential for $La_{0.15}Eu_{0.85}O$ and simple exponential for EuO.) (f) Relaxing asymmetry, A_r. The vertical dotted lines denote the Curie temperatures for EuO (68 K) and $La_{0.15}Eu_{0.85}O$ (96 K), with data for EuO taken from Ref. [5].

around T_C in $La_{0.15}Eu_{0.85}O$ that is less pronounced than that in pristine EuO (see Ref. [5]). Below T_C we note that $A_1/A_2 \sim 2$, which is the value anticipated for a polycrystalline ordered magnet. This ratio arises from a simple geometrical argument as the magnetic fields experienced by muons are powder averaged. Considering a fully ordered magnet: along two axes muons will precess about magnetic fields perpendicular to their spin, giving rise to the A_1 component, and along the remaining axis the field will be parallel to the muon spin and give rise to the A_2 component. In the paramagnetic phase the slowly relaxing A_2 component describes the whole signal. Using this we can estimate the fraction of the probed sample volume entering a magnetically ordered state at each temperature as $P_{mag} = 1.5 \times A_1/(A_1 + A_2)$. In Fig. 5(c) the static magnetic volume P_{mag} is shown as a function of temperature. These data show that quasistatic magnetic fields develop through the whole sample volume, within the $\sim 5\%$ measurement resolution, at T_C.

The wTF measurements at low temperature show a fast relaxation and a slowly relaxing oscillation, which can be attributed, respectively, to muons experiencing the large spontaneous fields and the weak applied field. This gives us another probe of the volume of the sample in which the muons are implanted that is magnetically ordered. To simplify the determination of this volume fraction we fitted the data omitting the first 0.25 μs to the function

$$A(t) = A_r \exp(-\sqrt{\eta t}) \cos(\gamma_\mu B + \phi). \quad (2)$$

This describes the slow relaxing precession of muons not experiencing large internal magnetic fields within the magnetic

volume of the sample. Before $0.25\,\mu$s the data in the ordered state are dominated by the fast relaxation from the magnetically ordered volume and so we used this cutoff to fit the slow relaxing precession consistently at all temperatures, following preliminary analysis to find the optimum cut-off value, which is the same as in Ref. [5]. The parameters η and B are shown in Figs. 5(d) and 5(e), respectively. The behavior of all three parameters is broadly similar to the equivalent parameters for EuO, except that transverse field relaxation here takes a square-root exponential form, rather than the simple exponential observed for EuO_{1-x}. This difference can be explained by the presence of an inhomogeneous distribution of fields at muon stopping sites due to nonmagnetic site dilution by the La-doping. The amplitude A_r [Fig. 5(f)] drops on entering the magnetically ordered phase, with the remaining amplitude being consistent with the background determined for the ZF measurements.

Both ZF and wTF data show that the sample suffers a sharp transition from a fully polarized state to a paramagnetic one. This behavior is similar to what we previously obtained for EuO_{1-x} [5]. If the sample did exhibit BMP, we would expect to observe phase separation that gradually develops from full magnetic order to full paramagnetism above the temperature at which long range order disappears. This is not observed. Therefore, we conclude that BMP could not be present in $La_{0.15}Eu_{0.85}O$ and the increase of T_C is a consequence of the existence of the RKKY-like interaction between the $4f$ and the $5d$ states.

IV. HALF-METALLICITY IN $LA_X EU_{1-x}O$

Of central interest in the EuO system is the half-metallic behavior below the Curie temperature. To investigate this as a function of La-doping density functional theory calculations were performed using the CASTEP plane-wave pseudopotential package [25]. As noted in our previous work [6], bulk EuO is poorly described by standard DFT employing local or semilocal functionals, which describe it as a paramagnetic metal instead of a ferromagnetic insulator. We use instead the DFT+U formalism [26], which augments the local spin density approximation with a Hubbard model description penalizing noninteger occupation of the Eu $4f$ orbitals. As in the previous work, we used $U = 7.3$ eV as it accurately reproduces both the experimental band gap and lattice parameter of bulk EuO. Simulations were performed with a plane-wave basis with a cutoff energy of 600 eV, and a Monkhorst-Pack k-point mesh with a minimum spacing of 0.1 Å^{-1}.

We first constructed a 64-atom supercell comprising $2 \times 2 \times 2$ copies of the eight-atom conventional cubic cell. Within this cell the calculated magnetic moment per Eu atom is exactly $7.0\mu_B$. La-doping was then introduced by substituting a chosen number of Eu atoms with La atoms and relaxing the resulting geometry.

Since La does not itself have occupied $4f$ states, each La substitution might be expected to reduce the overall magnetic moment by $7.0\mu_B$. However, in fact the magnitude of the reduction will be less than this, as the La acts as an electron donor to the $5d$ states comprising the conduction band. The lowest-lying conduction band (at Γ) is spin-split in the simulations by 0.7 eV due to the effective field from the

aligned Eu $4f$ moments. Therefore the electrons occupying the conduction band are at low concentration fully aligned with the magnetic moment of the $4f$ electrons. As the concentration increases, however, the minority-spin channel begins to be filled as well, and the contribution per conduction electron falls. At this point the half-metallicity is lost as the Fermi level crosses both majority- and minority-spin states, Fig. 6(c).

Figure 6 shows the effective band structure (EBS) of the La-doped supercell calculations, projected into the Brillouin zone of the conventional cubic unit cell of perfect EuO. We use the method of Popescu and Zunger [27] for the EBS plots, as implemented by Brommer *et al.* [28]. As the La-doping fraction x is increased, we see the Fermi level rise further into the conduction band around Γ. Simultaneously, the $4f$ bands become less distinct, as the La dopant atoms both disrupt the periodicity of the system and reduce its overall magnetic moment. At high x, we see evidence of subbands forming in many regions of the plot, but this is due to the artificial periodicity of the 64-atom cell and would not be observed so clearly for truly random distributions of defects in larger cells.

Mulliken population analysis using pseudoatomic orbitals as projectors indicates that the magnetic moment is not strongly localized on La sites. These only have a net spin in the range 0.1–$0.2\mu_B$ depending on the number of La atoms present in the cell. Instead, the net magnetic moment is distributed over the whole cell, indicating that it occupies rather delocalized $5d$ orbitals.

Given the high ordering temperature with Gd doping it is also opportune to compare the effects of La and Gd doping in order to better understand the phenomena of electron doping. We have therefore performed DFT calculations substituting a number of Eu atoms for Gd, and we show effective band structures from these simulations in Fig. 7. In comparison to the La-doped simulations, doping with Gd shows an overall similar behavior in relation to the position of the Fermi level with respect to the majority- and minority-spin bands, but the $4f$ density of states remains constant for increasing doping levels as there is no decrease in $4f$ occupancy per unit cell. Therefore, appropriate levels of Gd doping can also be expected to result in a half-metallic material.

V. VARIATION OF THE MAGNETIC MOMENT WITH La DOPING

To investigate the critical effect of the La-doping in EuO thin films one needs to understand the impact it has on the overall magnetic moment and also if any substantial changes occur in the band structure. The experimental determination of the magnetization of the $La_x Eu_{1-x}O$ films was done using low-temperature PNR on the neutron reflectometer CRISP at ISIS, UK, following preliminary measurements on beamline D17 at the ILL, France. The data analysis was performed by using the GenX [29] and XPolly fitting software. Figure 8 shows the PNR reflectivity obtained for the three measured $La_x Eu_{1-x}O$ samples at 5 K, showing that the 15% La-doping sample has a reduced magnetic moment of $5.7\mu_B$ per $La_{0.15}Eu_{0.85}O$ formula unit in comparison with the $6.98\mu_B$ per stoichiometric EuO formula unit.

Figure 9 compares the magnetic moment calculated using DFT and measured by PNR. The figure shows good agreement

FIG. 7. (Color online) Effective band structure for a 64-atom EuO supercell with 1 Gd substitutional atom (3.125%). The substitutional dopants on Eu sites are projected onto the eight-atom EuO conventional cell. The left panel corresponds to the majority-spin states and the right to the minority-spin states. The blue line is the Fermi level.

between the theory and the experiment at 10% doping. The 15% lanthanum doped EuO sample has a magnetic moment slightly reduced compared with the DFT calculation and we believe this is owing to the fact that the random distribution of the La atoms creates disorder that weakens the magnetic interactions. Another explanation is the presence of a small percentage of impurities lowering the overall magnetic moment measured by PNR. The figure also shows the calculated maximum and minimum possible polarization of the conduction band, in a model which assumes that at concentration x of La substituting Eu, the moment of the $4f$ electrons will be given by $7(1-x)\mu_B$. The maximum polarization curve assumes a further $x\mu_B$ contribution from fully polarized electrons in the conduction band, while the minimum polarization curve assumes they are fully

FIG. 6. (Color online) Effective band structure for a 64-atom EuO supercell: (a) Pristine EuO. (b) 1 La substitutional atom (3.125%). (c) Two La substitutional atoms (6.25%). (d) Three La substitutional atoms (9.375%). The La substitutional dopants on Eu sites are projected onto the eight-atom EuO conventional cell. The left panel corresponds to the majority-spin states and the right to the minority-spin states. The blue line is the Fermi level.

FIG. 8. (Color online) PNR data and analysis for the pristine EuO, 10% and 15% La doped EuO samples at 5 K. The spin-up and spin-down data is shown in red and blue, respectively.
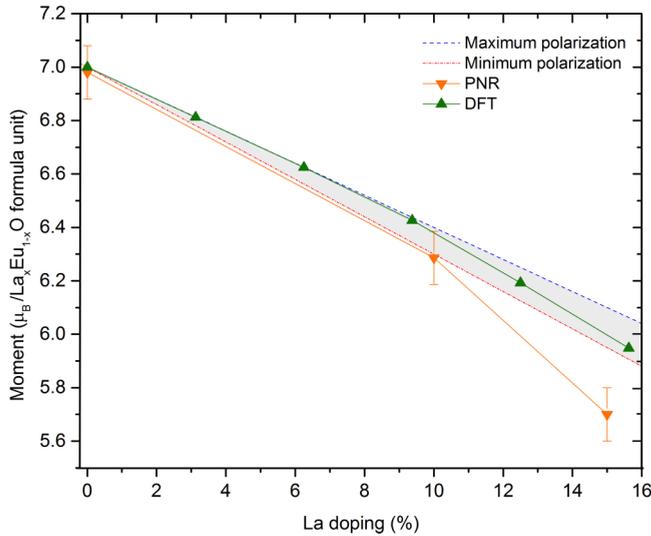
FIG. 9. (Color online) Comparison between the DFT calculations and the PNR analysis. The blue-dashed and red-dotted-dashed lines correspond to the maximum and minimum polarization coming from the doping electrons, respectively.

unpolarized. As explained before, the doping electrons populate only the majority-spin states at low doping levels. However as the doping increases, the Fermi energy is shifted upwards, crossing the minimum of the minority-spin conduction bands. Beyond this point both minority- and majority-spin states will be occupied and the overall polarization drops. This can be seen in Fig. 9: the DFT and maximum polarization curves start at similar values, and at about $x = 0.0625$ they begin to diverge. This divergence is attributed to the loss of the half-metallicity that occurs at $x = 0.031\,25$.

VI. CONCLUSIONS

In this paper we have shown that the La-doping acts like an n-dopant increasing the density of carriers in the $5d$ conduction band and strengthening the $4f$-$5d$ (Eu-Eu) interaction. The μSR experiments show that the electron doping in $La_x Eu_{1-x}O$ thin films has a similar effect on the magnetic properties to that which was found for EuO_{1-x}. One of the indicators is the fact that P_{mag} develops an abrupt transition at the elevated T_C

(96 K). This is a crucial indicator that there is no magnetic phase separation by the presence of bound magnetic polarons. It also indicates that no significant clustering of La is occurring, as this would broaden the transition. In the absence of bound magnetic polarons the electrons populate the $5d$ band and the RKKY-like interaction is the one that explains the T_C enhancement at high doping levels.

The PNR and DFT show a reduction of the overall magnetic moment of the $La_x Eu_{1-x}O$ formula unit. This is attributed to the replacement of Eu by La atoms reducing the total amount of $4f$ electrons in the system. The $4f$ electrons are responsible for carrying the magnetic moment and when removed a dilution of the total magnetic moment in the system occurs. The difference between the PNR and DFT at higher doping levels is ascribed to disorder and impurities in the sample.

The DFT calculations predict that the band structure remains almost unaffected for increasing doping where the only change is an upwards shift of the Fermi energy. For doping levels below 3.125% this change is just enough to make the Fermi energy intersect the majority-spin states leaving the minority-spin states unoccupied, forming a fully spin polarized conduction band. This half-metallic behavior occurs at much higher levels than the ones reported for oxygen deficient EuO, where at the same vacancy doping levels the system was already showing both the majority and minority channels occupied. The DFT calculations also show that the range of doping where half-metallicity can be expected in La- or Gd-doped EuO is limited by the size of the conduction band spin splitting. The presence of half-metallicity with La or Gd doping makes EuO an extraordinary system to study the phenomena of half-metallicity in strongly correlated systems.

[1] T. Dietl and H. Ohno, Rev. Mod. Phys. **86**, 187 (2014).

[2] A. Schmehl, V. Vaithyanathan, A. Herrnberger, S. Thiel, C. Richter, M. Liberati, T. Heeg, M. Rockerath, L. F. Kourkoutis, S. Muhlbauer, P. Boni, D. A. Muller, Y. Barash, J. Schubert, Y. Idzerda, J. Mannhart, and D. G. Schlom, Nat. Mater. **6**, 882 (2007).

[3] S. R. Dunsiger, J. P. Carlo, T. Goko, G. Nieuwenhuys, T. Prokscha, A. Suter, E. Morenzoni, D. Chiba, Y. Nishitani, T. Tanikawa, F. Matsukura, H. Ohno, J. Ohe, S. Maekawa, and Y. J. Uemura, Nat. Mater. **9**, 299 (2010).

[4] L. Passell, O. W. Dietrich, and J. Als-Nielsen, Phys. Rev. B **14**, 4897 (1976).

[5] P. M. S. Monteiro, P. J. Baker, A. Ionescu, C. H. W. Barnes, Z. Salman, A. Suter, T. Prokscha, and S. Langridge, Phys. Rev. Lett. **110**, 217208 (2013).

[6] M. Barbagallo, N. D. M. Hine, J. F. K. Cooper, N.-J. Steinke, A. Ionescu, C. H. W. Barnes, C. J. Kinane, R. M. Dalgliesh, T. R. Charlton, and S. Langridge, Phys. Rev. B **81**, 235216 (2010).

[7] G. Gütherodt, P. Wachter, and D. Imboden, Phys. Kondens. Mater. **12**, 292 (1971).

[8] T. S. Santos, J. S. Moodera, K. V. Raman, E. Negusse, J. Holroyd, J. Dvorak, M. Liberati, Y. U. Idzerda, and E. Arenholz, Phys. Rev. Lett. **101**, 147201 (2008).

[9] J. S. Moodera, T. S. Santos, and T. Nagahama, J. Phys.: Condens. Matter **19**, 165202 (2007).

[10] M. Barbagallo, T. Stollenwerk, J. Kroha, N.-J. Steinke, N. D. M. Hine, J. F. K. Cooper, C. H. W. Barnes, A. Ionescu, P. M. D. S. Monteiro, J.-Y. Kim, K. R. A. Ziebeck, C. J. Kinane, R. M. Dalgliesh, T. R. Charlton, and S. Langridge, Phys. Rev. B **84**, 075219 (2011).

[11] A. Melville, T. Mairoser, A. Schmehl, T. Birol, T. Heeg, B. Holländer, J. Schubert, C. J. Fennie, and D. G. Schlom, Appl. Phys. Lett. **102**, 062404 (2013).

[12] N. J. C. Ingle and I. S. Elfimov, Phys. Rev. B **77**, 121202 (2008).

[13] H. Ott, S. J. Heise, R. Sutarto, Z. Hu, C. F. Chang, H. H. Hsieh, H.-J. Lin, C. T. Chen, and L. H. Tjeng, Phys. Rev. B **73**, 094407 (2006).

[14] N. Jutong, U. Eckern, T. Mairoser, and U. Schwingenschlögl, Sci. Rep. **5**, 8038 (2015).

[15] H. Miyazaki, H. J. Im, K. Terashima, S. Yagi, M. Kato, K. Soda, T. Ito, and S. Kimura, Appl. Phys. Lett. **96**, 232503 (2010).

[16] D. T. Vigren, Phys. Rev. Lett. **41**, 194 (1978).

[17] A. Mauger and C. Godart, Phys. Rep. **141**, 51 (1986).

[18] K. Sattler and H. C. Siegmann, Phys. Rev. Lett. **29**, 1565 (1972).

[19] P. Liu and J. Tang, Phys. Rev. B **85**, 224417 (2012).

[20] A. Mauger, Phys. Status Solidi B **84**, 761 (1977).

[21] S. J. Blundell, T. Lancaster, F. L. Pratt, P. J. Baker, W. Hayes, J.-P. Ansermet, and A. Comment, Phys. Rev. B **81**, 092407 (2010).

[22] E. Morenzoni, H. Glucker, T. Prokscha, R. Khasanov, H. Luetkens, M. Birke, E. Forgan, C. Niedermayer, and M. Pleines, Nucl. Instrum. Meth. B **192**, 254 (2002).

[23] E. Morenzoni, T. Prokscha, A. Suter, H. Luetkens, and R. Khasanov, J. Phys.: Condens. Matter **16**, S4583 (2004).

[24] T. Prokscha, E. Morenzoni, K. Deiters, F. Foroughi, D. George, R. Kobler, A. Suter, and V. Vrankovic, Nucl. Instrum. Meth. A **595**, 317 (2008).

[25] S. J. Clark, M. D. Segall, C. J. Pickard, P. J. Hasnip, M. J. Probert, K. Refson, and M. C. Payne, Z. Kristallogr. **220**, 567 (2004).

[26] S. L. Dudarev, G. A. Botton, S. Y. Savrasov, C. J. Humphreys, and A. P. Sutton, Phys. Rev. B **57**, 1505 (1998).

[27] V. Popescu and A. Zunger, Phys. Rev. B **85**, 085201 (2012).

[28] P. Brommer and D. Quigley, J. Phys.: Condens. Matter **26**, 485501 (2014).

[29] M. Björck and G. Andersson, J. Appl. Crystallogr. **40**, 1174 (2007).